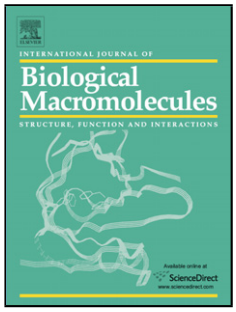

Title: Alzheimer's disease-associated ubiquitin mutant Ubb^{+1}: Properties of the carboxy-terminal domain and its influence on biomolecular interactions

Authors: Francesca Munari, Andrea Bortot, Michael Assfalg, Mariapina D'Onofrio

PII: S0141-8130(17)33065-9
DOI: https://doi.org/10.1016/j.ijbiomac.2017.11.121
Reference: BIOMAC 8601

To appear in: *International Journal of Biological Macromolecules*

Received date: 16-8-2017
Revised date: 17-11-2017
Accepted date: 19-11-2017

Please cite this article as: Francesca Munari, Andrea Bortot, Michael Assfalg, Mariapina D'Onofrio, Alzheimer's disease-associated ubiquitin mutant Ubb+1: Properties of the carboxy-terminal domain and its influence on biomolecular interactions, International Journal of Biological Macromolecules https://doi.org/10.1016/j.ijbiomac.2017.11.121

Alzheimer's disease-associated ubiquitin mutant Ubb^{+1}: properties of the carboxy-terminal domain and its influence on biomolecular interactions

Francesca Munari, Andrea Bortot, Michael Assfalg, and Mariapina D'Onofrio*

Department of Biotechnology, University of Verona, 37134 Verona (Italy)

Correspondence
Mariapina D'Onofrio
Department of Biotechnology, University of Verona, Strada Le Grazie 15, 37134 Verona (Italy)
Tel: +39 045 8027801, Fax: +39 045 8027929, E-mail: mariapina.d'onofrio@univr.it

Abstract

Ubb^{+1}, a ubiquitin (Ub) mutant protein originating from misreading of the Ub B gene, is found accumulated in brain tissues of Alzheimer's disease patients. The mutant attracts strong interest due to its possible participation in the molecular events leading to neurodegeneration. Ubb^{+1} is composed of the globular domain of Ub, linked to a 19-residue C-terminal peptide. Based on NMR relaxation and solvent accessibility measurements we obtained new insight into the molecular properties of Ubb^{+1}. We further determined the thermal stability of Ubb^{+1} in the monomeric form, and in Lys48- and Lys63-linked dimers. Finally, we explored the influence of the C-terminal fragment on the interactions of Ubb^{+1} with an isolated UBA2 domain and with membrane mimics.

Our data indicate that the C-terminal fragment of Ubb^{+1} is overall highly flexible, except for a short stretch which appears less solvent-exposed. While influencing the hydrodynamic properties of the globular domain, the fragment does not establish long-lived interactions with the globular domain. It results that the structure and stability of Ub are minimally perturbed by the peptide extension. However, binding to UBA2 and to membrane mimics are both affected, exemplifying possible changes in biomolecular recognition experienced by the disease-associated Ubb^{+1} compared to the wild-type protein.

Abbreviations

AD, Alzheimer's disease

CSP, chemical shift perturbation

DUB, deubiquitinating enzyme

hetNOE, heteronuclear nuclear Overhauser effects

HSQC, heteronuclear single quantum coherence

POPC, palmitoyl oleoyl phosphatidylcholine

POPG, palmitoyl oleoyl phosphatidylglycerol

PRE, paramagnetic relaxation enhancement

Ub, ubiquitin

UBA, ubiquitin associated

Keywords

Alzheimer's disease; NMR spectroscopy; protein dynamics; solvent accessibility; ubiquitin; Ubb^{+1}

1. Introduction

Ubiquitin (Ub) is a small and highly conserved protein that is covalently linked to protein targets to regulate numerous fundamental processes in eukaryotic cells, such as progression of cell cycle and division, DNA damage response, organelle biogenesis, protein trafficking, and protein turnover [1–3]. Ubiquitin conjugation, which consists in the formation of an isopeptide bond between the C-terminus of Ub and the ε-amino group of a specific lysine of the substrate protein, is accomplished by the sequential action of Ub-activating (E1), Ub-conjugating (E2), and Ub-ligating (E3) enzymes. Ub itself has seven lysine residues (Lys6, Lys11, Lys27, Lys29, Lys33, Lys48, Lys63) that can act as acceptor sites, leading to the formation of polyubiquitin (polyUb) chains endowed with a variety of linkage types and signaling functions. As an example, Lys48-chains mark substrates for rapid proteasomal degradation, while Lys63-chains play a role in endocytosis, DNA-damage response, cell signaling [1–3], and autophagic clearance of protein aggregates [4]. Ubiquitination is a reversible modification: a variety

of deubiquitinating enzymes (DUBs) hydrolyze Ub from the target protein, thereby remodeling or reversing the polyUb signal [5].

Dysfunction of Ub-related enzymes and pathways has been linked to the pathogenesis of severe human diseases, including Alzheimer's (AD), Parkinson's (PD), Huntington's (HD) diseases, Amyotrophic Lateral Sclerosis (ALS), cancer, metabolic syndromes, and genetic disorder [6–8]. In particular, a mutated version of Ub, named Ubb^{+1}, was found specifically accumulated in neurofibrillary tangles, neuropil threads and dystrophic neurites in brain tissues of AD patients [9]. Ubb^{+1} originates from misreading of the Ub B gene: the deletion of a dinucleotide adjacent to the GAGAG motif in the first repeat of the Ub transcript leads to the loss of Ub stop codon and the generation of a new one. This produces Ubb^{+1}, a Ub mutant protein where the carboxy(C)-terminal Gly76 is replaced by a tyrosine and linked to a 19-residue peptide [9]. Molecular misreading is a rare event that originates from mistakes of RNA polymerase II transcription activity, leading to generation of frameshift mRNA and protein mutants in the absence of genetic mutation. In physiological conditions, the Ub-proteasome system (UPS) well compensates for transcription errors by removing aberrant proteins through degradation. However, proteasomal degradation becomes progressively less efficient with aging, and accumulation of frameshift mutant proteins eventually occurs, such as in the case of AD [10].

Ubb^{+1} maintains the well-structured globular domain of Ub (Fig. 1) [11] and its lysine side chains can act as acceptors for polyUb chain linkage [11–14]. However, as a result of the lack of the C-terminal Gly76, Ubb^{+1} does not modify substrate proteins and instead terminates the elongation of polyUb chains. The resulting Ubb^{+1}-capped polyUb chains ($polyUbb^{+1}$) were shown to inhibit the proteasome [14,15], and were recalcitrant to disassembly mediated by DUBs [14]. Interestingly, it was shown that at low expression levels, Ubb^{+1} can be degraded by the 26S-proteasome, however after exceeding a threshold level of expression, Ubb^{+1} accumulates and inhibits the proteasome in a dose-dependent manner [16]. In neuroblastoma cells, overexpression of Ubb^{+1} leads to neuronal cell death [13]. Due to the essential function of the proteasome in protein turnover and clearance of misfolded proteins, the inhibition of proteasome by Ubb^{+1} species was proposed to be one of the key mechanisms of neuronal toxicity in AD. In particular, interaction of Ubb^{+1} with the enzyme E2-25K was suggested to modulate Aβ neurotoxicity via proteasomal inhibition [17]. Additionally, it was recently suggested that accumulation of extended Ub variants was due to their potent ability to inhibit specific DUBs [18].

Due to a possible participation of Ubb^{+1} in the molecular events leading to neurotoxicity and neurodegeneration in AD, there is large interest in elucidating the structural details of this frameshift

mutant Ub protein and the consequent functional differences with respect to the wild-type protein. In our work, we investigated structural and dynamic features of Ubb^{+1} using NMR spectroscopy methods that are particularly suited to explore protein molecules containing flexible domains such as the C-terminal extension of Ubb^{+1}. Calorimetry measurements were carried out to evaluate the contribution of the tail to the protein's thermal stability in both its monomeric and dimeric forms. Finally, the ability of Ubb^{+1} to interact with different biomolecules, in particular the UBA2 domain of the human homologue of the yeast DNA repair protein RAD23 (HHR23A) and membrane mimics, was here explored and characterized.

2. Materials and Methods

2.1 Materials

Deuterium oxide (99.9%), ^{13}C-glucose and $^{15}NH_4Cl$ were purchased from Spectra2000 s.r.l. (Roma, IT). Gadodiamide (gadolinium(III) 5,8-bis(carboxylatomethyl)-2-[2-(methylamino)-2-oxoethyl]-10-oxo-2,5,8,11-tetraazadodecane-1-carboxylate hydrate) was purchased from Selleck Chemicals. Powder cholesterol, phosphatidylglycerol and phosphatidylcholine were purchased from Sigma. 4,4-dimethyl-4-silapentane-1-sulfonic acid-d6 was purchased from Sigma.

2.2 Protein expression and purification

Recombinant human Ub and the UBA2 domain of HHR23A were expressed and purified as described previously [19]. Ub mutants K48R, K63R, and D77 were produced with the same protocol used for wild-type Ub. Human Ubb^{+1}, cloned in pET3 vector, was obtained from PCR extension of the human Ub sequence. The purification of Ubb^{+1} was performed with the same procedure as for Ub, with an additional size exclusion chromatography step.

Homogeneous di-ubiquitin chains (Ub_2) were obtained from Ub mutants, following the strategy described in [20], in overnight enzymatic reactions at 37 °C complemented with ATP, TCEP, and an ATP reconstituting cocktail. Recombinant human His-tagged E1 and GST-tagged E2-25K enzymes were used to obtain Lys48-linked Ub_2 products: Ub(K48R)-^{48}Ub(D77) and Ub(K48R)-$^{48}Ubb^{+1}$. Recombinant human His-tagged E1, yeast His-tagged Mms2 and yeast GST-tagged Ubc13 enzymes

were used for to produce Lys63-linked Ub_2 molecules: Ub(K63R)-^{63}Ub(D77) and Ub(K63R)-^{63}Ubb^{+1}. E2-25K, Mms2, and Ubc13 enzymes were produced in *Escherichia coli* BL21(DE3), while E1 was expressed in Rosetta cells. Purification of enzymes by affinity chromatography followed standard procedures. Ub_2 molecules were separated from unreacted Ub monomers by SP cation-exchange chromatography and further purified by size exclusion chromatography for calorimetry measurements.

Protein samples were concentrated using centrifugal filter units (Millipore).

2.3 Liposome preparation

Liposomes were obtained by dissolving cholesterol (Chl) and phosphatidylglycerol (POPG) or phosphatidylglycerol/phosphatidylcholine (POPG/POPC) phospholipids in chloroform/methanol (2:1, v/v) to form a homogeneous solution. A molar ratio of POPG/Chl 80:20 or POPG/POPC/Chl 40:40:20 was used to produce liposomes with different surface charge. The lipid mixture was then dried under nitrogen flux and the resulting lipid film dispersed in 10 mM potassium phosphate buffer at pH 6.8, to a final lipid concentration of ~120 mM. Vesicles were obtained by pressure extrusion with a hand-held miniextruder (Avanti, Alabaster, AL), by repeated passage through polycarbonate filters of 100 nm pore size, after pre-filtering through membranes of 1 μm and 400 nm pore sizes. The obtained liposomes had hydrodynamic diameter of 120 nm and polydispersity index < 0.1 as determined by dynamic light scattering (DLS) measurements performed with a Zetasizer Nano ZS instrument (Malvern Instruments, USA) at 25 °C.

2.4 NMR Spectroscopy

NMR experiments were acquired at 25 °C on a Bruker Avance III spectrometer, operating at ^{1}H Larmor frequency of 600.13 MHz, equipped with a triple resonance TCI cryogenic probe. NMR data were processed with Topspin 3.2 (Bruker) or NMRpipe [21] and analyzed with the software Sparky (T. D. Goddard and D. G. Kneller, University of California, San Francisco).

All samples for NMR measurements were prepared in 10 mM potassium phosphate aqueous buffer at pH 6.8, also containing protease inhibitors (Sigma) and 8% D_2O.

Sequence-specific backbone resonance assignment of Ubb^{+1} was obtained by analysis of CBCA(CO)NH, HNCACB, HNCO and HN(CA)CO spectra.

Secondary chemical shifts were calculated based on the random coil chemical shifts predicted by the Neighbor Corrected Structural Propensity Calculator [22] or the Camcoil software [23]. 4,4-dimethyl-4-silapentane-1-sulfonic acid-d_6 (DSS-d_6) was used for chemical shift referencing (0.0 ppm). Chemical shift perturbations were calculated as: $CSP = [(\Delta\delta_H)^2 + (\Delta\delta_N/5)^2]^{0.5}$, where $\Delta\delta_H$ and $\Delta\delta_N$ were the chemical shift changes measured in the ^1H and ^{15}N frequency dimensions, respectively.

^{15}N relaxation experiments were performed on 1 mM [^{15}N]Ubb^{+1} protein samples. ^{15}N longitudinal relaxation rates (R_1) were measured using relaxation delays in the range 0.01-1.26 s and ^{15}N transverse relaxation rates (R_2) were measured with relaxation delays in the range 8-224 ms. Steady-state {^1H}^{15}N heteronuclear nuclear Overhauser effects (hetNOE) were measured with a 6 s recycle delay. hetNOE values were calculated taking the ratio of peak intensities in saturated and reference spectra.

Transverse ^1H_N paramagnetic relaxation rate enhancements (PRE), ^1H_N-R_{2p}, were obtained from the difference in ^1H_N-R_2 measured on samples containing or not containing 2 mM gadodiamide. The measurements were performed as described previously [19]. Seven relaxation delays between 11.7 and 79 (60) ms were used in experiments acquired on samples without (with) 2 mM gadodiamide and the signal intensity decays were fitted to a single exponential function to obtain the corresponding rates.

The solvent accessibility of Ubb^{+1} backbone was also evaluated through measurement of exchange rates between water and NH protons by performing CLEANEX-PM-FHSQC experiments [24] using mixing times of 10, 25, 50, 75, 100, and 150 ms. The peak intensity (V), measured as a function of mixing time (x), was fitted according to the following equation $V/V_0 = k/(R_{1A,app}+k-R_{1B,app})\cdot\{\exp(-R_{1B,app}\cdot x)-\exp[-(R_{1A,app}+k)\cdot x]\}$ to obtain k, the normalized rate constant related to the exchange rate constant between NH protons and water [24]. V_0 is the intensity of the protein signals in a reference FHSQC experiment, $R_{1A,app}$ and $R_{1B,app}$ are apparent relaxation rates for protein and water, respectively. For $R_{1B,app}$ we used the value of 0.6 s^{-1}, in analogy with previous work [24].

The experimental rotational correlation time constant, τ_c, was obtained from ^{15}N relaxation data R_1, R_2, and hetNOE with the program ROTDIF [25]. Prediction of the τ_c of Ubb^{+1} was done with the HYCUD software [26,27]. First, we generated an ensemble of 1000 random structures with the EOM program [28], using the crystal structure of human Ub [29] and the human Ubb^{+1} sequence as input files. Next, we calculated the effective τ_c of the globular part of the full-length Ubb^{+1} with the HYCUD program [27]. By using AER of 2.9 Å and initial $\tau_{c,0}$ of 4.02 ns (our experimental value for Ub [19]), the algorithm predicted that the presence of a completely unrestricted C-terminal tail of Ubb^{+1} would

raise the τ_c value to 5.7 ± 1.0 ns.

The dissociation constant value for the Ubb^{+1}/UBA2 interaction was obtained by fitting experimental binding isotherms obtained from ^{1}H-^{15}N HSQC-based titration experiments, assuming a one-site binding model and by use of the Matlab program Kdfit [30]. The initial concentration of ^{15}N-Ubb^{+1} was 0.367 mM and that of the titrant UBA2 solution was 10 mM. The reported K_d value is the average of values determined from binding isotherms of seven residues using dilution-corrected protein concentrations.

2.5 Differential scanning calorimetry (DSC)

Thermal denaturation data were acquired with a Nano DSC instrument (TA Instruments Inc.). Samples were heated from 20 to 100 or 110 °C at a scan rate of 1 K min^{-1}. Selected experiments were also performed at 0.5 K min^{-1} to evaluate the scan rate dependence of the thermograms. Reheating runs were carried out to establish the operational reversibility of the thermal unfolding processes. Samples contained 0.05-0.1 mM protein dissolved in 100 mM sodium phosphate, pH 7.4, 100 mM NaCl. Before measurements, sample and reference solutions were properly degassed in an evacuated chamber for 10 minutes at room temperature and carefully loaded into the cells to avoid bubble formation. Calorimetric cells (operating volume 300 μL) were kept under a pressure of 3 atmospheres. Exhaustive cleaning of the cells was undertaken before each experiment. A background scan collected with buffer in both cells was subtracted from each scan. Analysis was performed using NanoAnalyze (TA Instruments Inc.). The calorimetric enthalpy was determined from the total peak integral after baseline correction. The thermal transition midpoint was determined as the temperature corresponding to the peak top.

3. Results and discussion

3.1 The C-terminal amino acids of Ubb^{+1} do not exhibit canonical secondary structure propensities

In a recent work, the NMR structure of Ubb^{+1} (incorporating eight exogenous residues at the N-terminus) was determined [11]. The structure shows a compact globular domain in the region 1-75, corresponding to the Ub moiety, while the remainder of the polypeptide chain is undefined due to the

lack of structural information (Fig. 1). However, a residual structure for residues 75-88 was proposed based on the larger values of heteronuclear NOE and smaller values of backbone RMSD in this region, compared to the rest of the terminal peptide [11].

To obtain further insight into the structural properties of the Ubb^{+1} 19-residue extension, we measured secondary chemical shifts, a very sensitive parameter used to probe local conformation [31,32] and structural propensities in unfolded proteins [33]. We thus assigned the backbone resonances of Ubb^{+1}, produced in the absence of affinity tags, by using a series of standard 3D heteronuclear NMR experiments. Then, we calculated secondary chemical shifts as the difference between Ubb^{+1} $^{13}C\alpha$ or $^{13}C'$ chemical shifts and the corresponding random coil values [22,23]. Data shown in Fig. 2 indicate that both $^{13}C'$ and $^{13}C\alpha$ secondary chemical shifts closely match the α and β structures of the globular region of Ubb^{+1}. By contrast, secondary chemical shift values are very close to zero for the 19-residue extension, indicating the absence of α and β secondary structure propensities. This finding was validated by the use of two independent datasets of random coil values [22,23].

3.2 The middle region of the C-terminal domain displays reduced solvent accessibility and mobility

^{15}N-spin relaxation rate constants, R_1 and R_2, and steady state heteronuclear NOE were measured to investigate the backbone dynamics of the 19-residue extension. Data reported in Fig. 3 reflect the modular architecture of the protein: the first region (residues 1-72) reports on the relatively rigid nature of the globular Ub domain, while the C-terminal tail is characterized by increased backbone mobility. From ^{15}N relaxation data of Ubb^{+1}, we estimated a rotational correlation time constant (τ_c) for the globular domain of 5.77 ± 0.04 ns, much higher than the value of 4.02 ns estimated for Ub [19]. However, the determined τ_c value is in excellent agreement with the value of 5.7 ± 1.0 ns predicted using the HYCUD approach [27]. The prediction was made considering a completely unrestricted mobility of the C-terminal tail of Ubb^{+1} which exerts a dragging effect on the globular part *via* hydrodynamic coupling. The coincidence of experimental and predicted values strongly suggested that interactions between the two protein domains were absent.

While displaying overall larger backbone flexibility, the C-terminal tail did not exhibit uniform dynamics, in agreement with previous conclusions [11]. Of particular interest were residues Asp84 and Arg85, which showed $\{^1H\}^{15}N$-NOE (hetNOE) values that departed from the decreasing trend of the

rest of residues in the C-terminal tail (Fig. 3A), suggesting the presence of reduced local backbone mobility. Interestingly, this feature was in qualitative agreement with the degree of solvent accessibility determined by two alternative approaches. In a first approach, we measured amide ^{1}H paramagnetic relaxation enhancements (PRE) in the presence of the soluble paramagnetic agent gadodiamide (Gd-DTPA-BMA) [34]. Fig. 4A shows the transverse PRE, ^1H_N-R_{2p}, as a function of the amino acid sequence. Data referred to the first part, 1-75, were in agreement with what found previously for Ub [19], with residues 8-14, 45-49, and 72-75 showing large ^1H_N-R_{2p} values, indicative of high accessibility to the paramagnetic cosolute. Interestingly, the 19-residue extension experienced large PRE, although non-uniformly distributed along the chain and with a marked dip in the region 78-88 (^1H_N-R_{2p} < 30 s^{-1}). Therefore, this region appeared less exposed to the solvent than the rest of the tail. The most protected residues of the tail were Asp82, Asp84 and Arg85, exhibiting PRE values of 13.9 ± 0.8 s^{-1}, 14.3 ± 0.3 s^{-1}, and 14.3 ± 0.5 s^{-1}.

To support these conclusions, we performed an independent measurement of amide proton exchange with bulk solvent based on the CLEANEX-PM-FHSQC experiment. In this NMR experiment, solvent accessibility was probed by monitoring water-protein proton exchange taking place during a mixing time which followed a selective water resonance excitation [24]. Fig. 4B shows the determined water-amide proton exchange rates, k, against the Ubb^{+1} sequence. The majority of residues belonging to the globular part were protected from exchange with solvent and therefore did not show measurable signals after the given mixing times. However, resonances corresponding to residues 8-12, 39, 46, 47, 49, 63, and residues within the C-terminal tail were observable, indicative of a significant degree of solvent accessibility. For these residues, we determined the water-amide proton exchange rates. In the 19-residues extension, amino acids 78-87 exhibited the smallest k value (k < 8 s^{-1}), confirming that this part of the C-terminal tail was less exposed to the solvent. In particular, the experiment confirmed that residues Asp84 and Arg85, showing k values of 0.9 ± 0.1 s^{-1} and 1.2 ± 0.1 s^{-1}, were the least solvent-accessible residues of the C-terminal peptide.

3.2 Ubb^{+1} displays similar thermal stability as Ub in both monomeric and dimeric species

To determine if the 19-residue extension affected the thermal stability of Ub, differential scanning calorimetry (DSC) experiments were performed. Ub is a highly compact globular protein which

undergoes thermal unfolding at elevated temperature [35,36]. According to previous investigations, the denaturation mechanism corresponds to a fully reversible two-state transition when Ub is dissolved in acidic solution [35]. The thermal transition was also found to be reversible in PBS solution, pH 7.4 [37], however some authors reported the onset of protein aggregation and significantly reduced reversibility in neutral pH solution [35,38]. The thermal unfolding of both Lys63- and Lys48-Ub_2 was found to be irreversible [37]. In our work, we established the calorimetric irreversibility of Ub_2 thermal unfolding and the partial reversibility (~30%) of Ub denaturation (Supplementary Fig. S1). The temperature of the peak maximum for Ub displayed an increase of less than 0.5 K when changing the scan rate from 0.5 K min^{-1} to 1 K min^{-1}, indicating little sensitivity of the endotherm to kinetic constraints. However, a slight concentration dependence of the thermograms was observed in the range 50-100 μM. Thus, comparative analyses between wild type and variant proteins were performed at equal scan rates on samples containing identical protein concentrations. To avoid the assumptions or simplifications inherent in model-based analyses, we limited our investigation to a phenomenological analysis of the experimental data (measured calorimetric parameters are reported in Supplementary Table S1). Indeed, the midpoint of thermal unfolding curves provides an adequate indication of the relative thermal stability of related proteins.[39]

DSC data indicated that the apparent thermal transition midpoint of Ubb^{+1} was unchanged with respect to that of Ub (T_m = 369 K)(Fig. 5 and Table S1). The calorimetric enthalpy values of the two variants differed by 5% (Table S1), which is in the order of experimental uncertainty. Thus, the terminal polypeptide had essentially no influence on the thermal stability of the globular domain. We further inspected the thermal behaviour of Ub_2 molecules. In agreement with previous work [35], our experiments indicated a decreased thermal transition midpoint of both dimeric Ub-^{63}Ub (T_m = 353 K) and Ub-^{48}Ub (T_m = 358 K)(Fig. 5 and Table S1). Because of the reported formation of amyloid-like fibril assemblies [35], the stability of polyUb chains is of utmost relevance in the context of neurodegenerative diseases. Here, we found that substitution of Ub with Ubb^{+1} did not perturb the thermal transition of dimeric species and the change in calorimetric enthalpy was less than 5%, again indicating that the C-terminal tail of Ubb^{+1} does not interact with the globular units. In this respect, it should be noted that Ub-Ubb^{+1} dimers are structurally similar to their wild-type counterparts [12], therefore no changes are introduced by the extension on the intersubunit interfaces. Apparently, the conjugation of the terminal peptide to the flexible C-terminus of Ub has no influence on the

intramolecular interactions that govern the folding/unfolding process.

3.3 The affinity of Ubb^{+1} for (HHR23A)UBA2 is enhanced compared to that of Ub

To investigate the influence of the C-terminal extension in Ubb^{+1} on biomolecular recognition, we carried out a binding experiment with a model Ub protein partner: the Ub-associated C-terminal domain (UBA2) of the human homologue of the yeast DNA repair protein Rad23 (HHR23A). Rad23, originally recognized as an important player in nucleotide excision repair, mediates targeting of ubiquitinated proteins to the proteasome for degradation [40]. Ubb^{+1}/UBA2 titration experiments monitored by ^{1}H-^{15}N HSQC spectra were carried out to describe the UBA2 interaction surface on Ubb^{+1} and to estimate the dissociation constant, K_d. Fig. 6A shows the chemical shift perturbation (CSP) profile of Ubb^{+1} resonances upon binding to UBA2. The most affected regions are centered on residues Leu8, Ile44, and Val70, which form the well-known hydrophobic patch of the Ub surface, involved in several recognition events. The perturbation profile is highly similar to that determined for Ub upon binding to UBA2 [19] suggesting that the supramolecular arrangement was preserved, and for Ubb^{+1} binding to E2-25K enzyme which contains a UBA domain [11]. We found that the 19-residue extension did not experience perturbations, except for residues Glu81 and Asp82, for which a small effect was detected. The analysis of binding isotherms based on CSP data (Fig. 6B) revealed that the affinity of the Ubb^{+1}/UBA2 complex (K_d = 305 ± 18 μM) was slightly larger than that previously determined for the Ub/UBA2 system (K_d = 412 ± 52 μM) [19]. This result is consistent with previous findings on the interaction between E2-25K and Ubb^{+1}, which was found to be stronger than that of E2-25K and Ub. The observed increased affinity could be due to a slightly extended interaction surface area in the minimum-energy complex and/or to enhanced probability of formation of encounter complexes due to transient anchoring of the flexible tail.

3.4 C-terminal amino acids hinder adsorption of Ubb^{+1} to anionic lipid vesicles

Recently, it was shown that Ub binds transiently to liposomes through its hydrophobic patch and adjacent positively charged residues [41]. This finding is of interest considering that transient interactions between Ub and membranes might take place within cells due to the key role of Ub in regulating the sorting of membrane proteins [42] and autophagic processes [43]. Moreover, liposomes

have been widely used as membrane mimics to investigate the interaction between proteins and membranes [31,44–46] We thus explored whether the 19-residue extension of Ubb^{+1} could affect the Ub/liposome interaction using an NMR-based binding assay where a series of ^{1}H-spectra of Ub or Ubb^{+1} were acquired in the presence of increasing amounts of negatively charged liposomes. Fig. 6C shows that the amide ^{1}H signal envelope, integrated in the region between 9.0 and 9.8 ppm, progressively decreases as the protein molecules bind to the negatively charged liposomes made of POPG and cholesterol at a molar ratio of 80:20. In comparison to Ub, the signal intensity loss displayed by Ubb^{+1} was much less pronounced, indicating a substantially reduced affinity. Similarly, Ub experienced weak binding affinity to liposomes bearing reduced negative charge (composed of POPG, POPC and cholesterol at 40:40:20 molar ratio), while almost no interaction was observed between these liposomes and Ubb^{+1}. Clearly, electrostatic attraction plays a fundamental role in the formation of protein-liposome assemblies, therefore it seems likely that the reduced affinity of Ubb^{+1} was due to the acidic character of the C-terminal peptide (the calculated pI for residues Y76-Q95 is 4.7). Thus, translocation of Ubb^{+1} (and of polyUb chains terminated by Ubb^{+1}) within the cellular milieu and in proximity to lipid membranes may be significantly different compared to the wild-type species, possibly resulting in perturbed intracellular communication.

4. Conclusions

Our findings support the notion that the 19-residue extension of Ubb^{+1} lacks a well ordered structure and persistent canonical secondary structure elements. However, we observed that the flexible fragment displayed non-uniform structural and dynamic properties along its amino acid sequence. In particular, the region Asp78-Asp87 was characterized by diminished solvent exposure, with Asp84 and Arg85 being the most protected residues against proton exchange with bulk solvent and among the less accessible to a paramagnetic molecular probe. The relatively larger hetNOE values of Asp84 and Arg85, compared to adjacent residues, further indicated that the polypeptide backbone in those positions experienced reduced mobility on the ps-ns timescale. From analysis of global dynamics based on ^{15}N-spin relaxation data, it emerged that the mobility of the C-terminal tail was independent from that of the globular domain, and persistent interdomain interactions were absent. Hence, it is possible that a reduction in local flexibility might originate from structural constraints imposed by the sequence of amino acids, and in particular by the proximity of two proline residues (Pro83 and Pro90).

Consistently with the above picture and with the absence of structural perturbations, inferred from chemical shift analysis, the peptide extension did not affect the protein thermal stability in either monomeric or dimeric species. However, biomolecular recognition was in part perturbed: the interaction of Ubb^{+1} with (HHR23A)UBA2 was characterized by enhanced affinity compared to that of Ub, and the weak association of Ub with anionic lipid surfaces was significantly reduced in the case of the variant.

It can be concluded that the globular architecture of Ub is sufficiently robust not to be particularly influenced by the unintended covalent conjugation of a peptide to its flexible C-terminus. However, the presence of a fragment that extends by 25% beyond the regular polypeptide length is certainly not without consequences, and the selected interactions investigated in our work exemplify possible changes in biomolecular recognition and diffusive dynamics experienced by disease-associated mutant Ub species, compared to wild-type molecules, in physio(patho)logical conditions.

Conflicts of interest

The authors declare no conflict of interest.

Acknowledgments

This work was supported by the University of Verona (Progetto Ricerca di Base 2015, to M.D.). F.M. thanks “Fondazione Umberto Veronesi” for granting a postdoctoral fellowship. We acknowledge "Centro Piattaforme Tecnologiche" of the University of Verona for giving access to NMR, DLS, and DSC instrumentation. We thank Prof. Dimitrios Fessas for useful discussions.

References

[1] D. Komander, The emerging complexity of protein ubiquitination, Biochem. Soc. Trans. 37 (2009) 937–953. doi:10.1042/BST0370937.

[2] C.M. Pickart, D. Fushman, Polyubiquitin chains: polymeric protein signals, Curr. Opin. Chem. Biol. 8 (2004) 610–616. doi:10.1016/j.cbpa.2004.09.009.

[3] J.-F. Trempe, Reading the ubiquitin postal code, Curr. Opin. Struct. Biol. 21 (2011) 792–801. doi:10.1016/j.sbi.2011.09.009.

[4] J.M.M. Tan, E.S.P. Wong, D.S. Kirkpatrick, O. Pletnikova, H.S. Ko, S.-P. Tay, M.W.L. Ho, J. Troncoso, S.P. Gygi, M.K. Lee, V.L. Dawson, T.M. Dawson, K.-L. Lim, Lysine 63-linked ubiquitination promotes the formation and autophagic clearance of protein inclusions associated with neurodegenerative diseases, Hum. Mol. Genet. 17 (2008) 431–439. doi:10.1093/hmg/ddm320.

[5] T.E.T. Mevissen, D. Komander, Mechanisms of Deubiquitinase Specificity and Regulation, Annu. Rev. Biochem. (2017). doi:10.1146/annurev-biochem-061516-044916.

[6] G. Atkin, H. Paulson, Ubiquitin pathways in neurodegenerative disease, Front. Mol. Neurosci. 7 (2014) 63. doi:10.3389/fnmol.2014.00063.

[7] Q. Huang, M.E. Figueiredo-Pereira, Ubiquitin/proteasome pathway impairment in neurodegeneration: therapeutic implications, Apoptosis Int. J. Program. Cell Death. 15 (2010) 1292–1311. doi:10.1007/s10495-010-0466-z.

[8] D. Popovic, D. Vucic, I. Dikic, Ubiquitination in disease pathogenesis and treatment, Nat. Med. 20 (2014) 1242–1253. doi:10.1038/nm.3739.

[9] F.W. van Leeuwen, D.P. de Kleijn, H.H. van den Hurk, A. Neubauer, M.A. Sonnemans, J.A. Sluijs, S. Köycü, R.D. Ramdjielal, A. Salehi, G.J. Martens, F.G. Grosveld, J. Peter, H. Burbach, E.M. Hol, Frameshift mutants of beta amyloid precursor protein and ubiquitin-B in Alzheimer's and Down patients, Science. 279 (1998) 242–247.

[10] X. Chen, D. Petranovic, Role of frameshift ubiquitin B protein in Alzheimer's disease, Wiley Interdiscip. Rev. Syst. Biol. Med. 8 (2016) 300–313. doi:10.1002/wsbm.1340.

[11] S. Ko, G.B. Kang, S.M. Song, J.-G. Lee, D.Y. Shin, J.-H. Yun, Y. Sheng, C. Cheong, Y.H. Jeon, Y.-K. Jung, C.H. Arrowsmith, G.V. Avvakumov, S. Dhe-Paganon, Y.J. Yoo, S.H. Eom, W. Lee, Structural basis of E2-25K/UBB+1 interaction leading to proteasome inhibition and neurotoxicity, J. Biol. Chem. 285 (2010) 36070–36080. doi:10.1074/jbc.M110.145219.

[12] M. Chojnacki, D. Zhang, M. Talarowska, P. Gałecki, J. Szemraj, D. Fushman, M.A. Nakasone, Characterizing polyubiquitinated forms of the neurodegenerative ubiquitin mutant UBB(+1), FEBS Lett. 590 (2016) 4573–4585. doi:10.1002/1873-3468.12484.

[13] F.M. De Vrij, J.A. Sluijs, L. Gregori, D.F. Fischer, W.T. Hermens, D. Goldgaber, J. Verhaagen, F.W. Van Leeuwen, E.M. Hol, Mutant ubiquitin expressed in Alzheimer's disease causes neuronal death, FASEB J. Off. Publ. Fed. Am. Soc. Exp. Biol. 15 (2001) 2680–2688. doi:10.1096/fj.01-0438com.

[14] Y.A. Lam, C.M. Pickart, A. Alban, M. Landon, C. Jamieson, R. Ramage, R.J. Mayer, R. Layfield, Inhibition of the ubiquitin-proteasome system in Alzheimer's disease, Proc. Natl. Acad. Sci. U. S. A. 97 (2000) 9902–9906. doi:10.1073/pnas.170173897.

[15] K. Lindsten, F.M.S. de Vrij, L.G.G.C. Verhoef, D.F. Fischer, F.W. van Leeuwen, E.M. Hol, M.G. Masucci, N.P. Dantuma, Mutant ubiquitin found in neurodegenerative disorders is a ubiquitin fusion degradation substrate that blocks proteasomal degradation, J. Cell Biol. 157 (2002) 417–427. doi:10.1083/jcb.200111034.

[16] P. van Tijn, F.M.S. de Vrij, K.G. Schuurman, N.P. Dantuma, D.F. Fischer, F.W. van Leeuwen,

E.M. Hol, Dose-dependent inhibition of proteasome activity by a mutant ubiquitin associated with neurodegenerative disease, J. Cell Sci. 120 (2007) 1615–1623. doi:10.1242/jcs.03438.
[17] S. Song, S.-Y. Kim, Y.-M. Hong, D.-G. Jo, J.-Y. Lee, S.M. Shim, C.-W. Chung, S.J. Seo, Y.J. Yoo, J.-Y. Koh, M.C. Lee, A.J. Yates, H. Ichijo, Y.-K. Jung, Essential role of E2-25K/Hip-2 in mediating amyloid-beta neurotoxicity, Mol. Cell. 12 (2003) 553–563.
[18] D. Krutauz, N. Reis, M.A. Nakasone, P. Siman, D. Zhang, D.S. Kirkpatrick, S.P. Gygi, A. Brik, D. Fushman, M.H. Glickman, Extended ubiquitin species are protein-based DUB inhibitors, Nat. Chem. Biol. 10 (2014) 664–670. doi:10.1038/nchembio.1574.
[19] F. Munari, A. Bortot, S. Zanzoni, M. D'Onofrio, D. Fushman, M. Assfalg, Identification of primary and secondary UBA footprints on the surface of ubiquitin in cell-mimicking crowded solution, FEBS Lett. 591 (2017) 979–990. doi:10.1002/1873-3468.12615.
[20] C.M. Pickart, S. Raasi, Controlled synthesis of polyubiquitin chains, Methods Enzymol. 399 (2005) 21–36. doi:10.1016/S0076-6879(05)99002-2.
[21] F. Delaglio, S. Grzesiek, G.W. Vuister, G. Zhu, J. Pfeifer, A. Bax, NMRPipe: a multidimensional spectral processing system based on UNIX pipes, J. Biomol. NMR. 6 (1995) 277–293.
[22] K. Tamiola, B. Acar, F.A.A. Mulder, Sequence-specific random coil chemical shifts of intrinsically disordered proteins, J. Am. Chem. Soc. 132 (2010) 18000–18003. doi:10.1021/ja105656t.
[23] A. De Simone, A. Cavalli, S.-T.D. Hsu, W. Vranken, M. Vendruscolo, Accurate random coil chemical shifts from an analysis of loop regions in native states of proteins, J. Am. Chem. Soc. 131 (2009) 16332–16333. doi:10.1021/ja904937a.
[24] T.L. Hwang, P.C. van Zijl, S. Mori, Accurate quantitation of water-amide proton exchange rates using the phase-modulated CLEAN chemical EXchange (CLEANEX-PM) approach with a Fast-HSQC (FHSQC) detection scheme, J. Biomol. NMR. 11 (1998) 221–226.
[25] O. Walker, R. Varadan, D. Fushman, Efficient and accurate determination of the overall rotational diffusion tensor of a molecule from (15)N relaxation data using computer program ROTDIF, J. Magn. Reson. San Diego Calif 1997. 168 (2004) 336–345. doi:10.1016/j.jmr.2004.03.019.
[26] N. Rezaei-Ghaleh, F. Klama, F. Munari, M. Zweckstetter, Predicting the rotational tumbling of dynamic multidomain proteins and supramolecular complexes, Angew. Chem. Int. Ed Engl. 52 (2013) 11410–11414. doi:10.1002/anie.201305094.
[27] N. Rezaei-Ghaleh, F. Klama, F. Munari, M. Zweckstetter, HYCUD: a computational tool for prediction of effective rotational correlation time in flexible proteins, Bioinforma. Oxf. Engl. 31 (2015) 1319–1321. doi:10.1093/bioinformatics/btu824.
[28] P. Bernadó, E. Mylonas, M.V. Petoukhov, M. Blackledge, D.I. Svergun, Structural characterization of flexible proteins using small-angle X-ray scattering, J. Am. Chem. Soc. 129 (2007) 5656–5664. doi:10.1021/ja069124n.
[29] S. Vijay-Kumar, C.E. Bugg, W.J. Cook, Structure of ubiquitin refined at 1.8 A resolution, J. Mol. Biol. 194 (1987) 531–544.
[30] R. Varadan, M. Assfalg, A. Haririnia, S. Raasi, C. Pickart, D. Fushman, Solution conformation of Lys63-linked di-ubiquitin chain provides clues to functional diversity of polyubiquitin signaling, J. Biol. Chem. 279 (2004) 7055–7063. doi:10.1074/jbc.M309184200.
[31] R. Bajaj, F. Munari, S. Becker, M. Zweckstetter, Interaction of the intermembrane space domain of Tim23 protein with mitochondrial membranes, J. Biol. Chem. 289 (2014) 34620–34626. doi:10.1074/jbc.M114.595702.
[32] F. Munari, N. Rezaei-Ghaleh, S. Xiang, W. Fischle, M. Zweckstetter, Structural plasticity in human heterochromatin protein 1β, PloS One. 8 (2013) e60887. doi:10.1371/journal.pone.0060887.
[33] M.D. Mukrasch, S. Bibow, J. Korukottu, S. Jeganathan, J. Biernat, C. Griesinger, E.

Mandelkow, M. Zweckstetter, Structural polymorphism of 441-residue tau at single residue resolution, PLoS Biol. 7 (2009) e34. doi:10.1371/journal.pbio.1000034.
[34] H.G. Hocking, K. Zangger, T. Madl, Studying the structure and dynamics of biomolecules by using soluble paramagnetic probes, Chemphyschem Eur. J. Chem. Phys. Phys. Chem. 14 (2013) 3082–3094. doi:10.1002/cphc.201300219.
[35] P.L. Wintrode, G.I. Makhatadze, P.L. Privalov, Thermodynamics of ubiquitin unfolding, Proteins Struct. Funct. Genet. 18 (1994) 246–253. doi:10.1002/prot.340180305.
[36] G.I. Makhatadze, M.M. Lopez, J.M. Richardson, S.T. Thomas, Anion binding to the ubiquitin molecule, Protein Sci. Publ. Protein Soc. 7 (1998) 689–697. doi:10.1002/pro.5560070318.
[37] D. Morimoto, E. Walinda, H. Fukada, Y.-S. Sou, S. Kageyama, M. Hoshino, T. Fujii, H. Tsuchiya, Y. Saeki, K. Arita, M. Ariyoshi, H. Tochio, K. Iwai, K. Namba, M. Komatsu, K. Tanaka, M. Shirakawa, The unexpected role of polyubiquitin chains in the formation of fibrillar aggregates, Nat. Commun. 6 (2015) 6116. doi:10.1038/ncomms7116.
[38] G. Arena, R. Fattorusso, G. Grasso, G.I. Grasso, C. Isernia, G. Malgieri, D. Milardi, E. Rizzarelli, Zinc(II) Complexes of Ubiquitin: Speciation, Affinity and Binding Features, Chem. - Eur. J. 17 (2011) 11596–11603. doi:10.1002/chem.201101364.
[39] C.N. Pace, J.M. Scholtz, Measuring the conformational stability of a protein, in T.E. Creighton, ed., Protein structure: a practical approach, 2nd ed., repr, IRL Press, Oxford, 2002.
[40] N.P. Dantuma, C. Heinen, D. Hoogstraten, The ubiquitin receptor Rad23: at the crossroads of nucleotide excision repair and proteasomal degradation, DNA Repair. 8 (2009) 449–460. doi:10.1016/j.dnarep.2009.01.005.
[41] A. Ceccon, V. Tugarinov, A. Bax, G.M. Clore, Global Dynamics and Exchange Kinetics of a Protein on the Surface of Nanoparticles Revealed by Relaxation-Based Solution NMR Spectroscopy, J. Am. Chem. Soc. 138 (2016) 5789–5792. doi:10.1021/jacs.6b02654.
[42] L. Hicke, R. Dunn, Regulation of membrane protein transport by ubiquitin and ubiquitin-binding proteins, Annu. Rev. Cell Dev. Biol. 19 (2003) 141–172. doi:10.1146/annurev.cellbio.19.110701.154617.
[43] A. Khaminets, C. Behl, I. Dikic, Ubiquitin-Dependent And Independent Signals In Selective Autophagy, Trends Cell Biol. 26 (2016) 6–16. doi:10.1016/j.tcb.2015.08.010.
[44] A. Ceccon, M. D'Onofrio, S. Zanzoni, D.L. Longo, S. Aime, H. Molinari, M. Assfalg, NMR investigation of the equilibrium partitioning of a water-soluble bile salt protein carrier to phospholipid vesicles, Proteins. 81 (2013) 1776–1791. doi:10.1002/prot.24329.
[45] M. Pedò, F. Löhr, M. D'Onofrio, M. Assfalg, V. Dötsch, H. Molinari, NMR studies reveal the role of biomembranes in modulating ligand binding and release by intracellular bile acid binding proteins, J. Mol. Biol. 394 (2009) 852–863. doi:10.1016/j.jmb.2009.10.014.
[46] M. D'Onofrio, S. Zanzoni, F. Munari, H.L. Monaco, M. Assfalg, S. Capaldi, The long variant of human ileal bile acid-binding protein associated with colorectal cancer exhibits sub-cellular localization and lipid binding behaviour distinct from those of the common isoform, Biochim. Biophys. Acta BBA - Gen. Subj. 1861 (2017) 2315–2324. doi:10.1016/j.bbagen.2017.07.004.

FIGURE CAPTIONS

Fig. 1. *Illustration of the structure of Ubb^{+1}.* Cartoon representation of the five lowest energy NMR structures of Ubb^{+1} (PDB 2KX0, [11]). The globular domain is colored in orange, the C-terminal 19-residue fragment is shown in green. The eight exogenous N-terminal residues are not displayed as they are absent in our Ubb^{+1} construct.

Fig. 2. *Analysis of Ubb^{+1} chemical shifts*. Secondary ^{13}C' (A) and ^{13}Cα (B) chemical shifts ($\Delta\delta^{13}$C' and $\Delta\delta^{13}$Cα) of Ubb^{+1}, obtained with Camcoil random coil values, are plotted versus the protein sequence. Secondary ^{13}C' (C) and ^{13}Cα (D) chemical shifts ($\Delta\delta^{13}$C' and $\Delta\delta^{13}$Cα) of Ubb^{+1}, obtained with the Neighbor Corrected Structural Propensity Calculator random coil values, are plotted versus the protein sequence.

Fig. 3. *Analysis of Ubb^{+1} backbone dynamics*. ^{15}N–spin relaxation rates of [^{15}N]Ubb^{+1} are shown as a function of residue number: A) steady-state {^{1}H}^{15}N heteronuclear NOE (hetNOE); B) R_2 and C) R_1. Residues affected by signal overlap or with insufficient signal-to-noise ratio were excluded from the analysis.

Fig. 4. *Solvent accessibility of Ubb^{+1}*. The solvent exposure of Ubb^{+1} has been probed by solvent PRE (A) or by measurement of water-amide proton exchange rates (B). In A) the $^{1}H_N$-R_{2p} rates of Ubb^{+1} obtained with 2 mM gadodiamide are plotted as a function of protein sequence. In B) the water-amide proton exchange rates (k) measured through a CLEANEX-PM-FHSQC experiment are reported versus the protein sequence. Error bars are standard errors obtained from data fitting. Residues affected by signal overlap or with insufficient signal-to-noise ratio were excluded from the analysis.

Fig. 5. *Thermal stability measured by calorimetry*. Differential scanning calorimetry thermograms recorded on samples of A) Ub, black, Ubb^{+1}, orange, B) Ub-^{48}Ub, black, Ub-^{48}Ubb^{+1}, orange, C) Ub-^{63}Ub, black, Ub-^{63}Ubb^{+1}, orange. DSC traces are baseline-corrected.

Fig. 6. *Biomolecular interactions of Ubb^{+1}*. A) Plot of the chemical shift perturbations (CSP)

determined from $^{1}H,^{15}N$-HSQC spectra recorded on [^{15}N]Ubb^{+1} in the presence of (HHR23A)UBA2 at 1:7 molar ratio and in the absence of UBA2. B) Binding isotherms for selected Ubb^{+1} residues based on CSP data from a UBA2/ Ubb^{+1} NMR titration experiment. C) Binding of Ubb^{+1} or Ub to liposomes monitored through analysis of protein ^{1}H signal intensity loss as a function of total lipids to protein molar ratio. Titration data for Ub/POPG-Chl 80:20 (blue), Ubb^{+1}/POPG-Chl 80:20 (red), Ub/POPG-POPC-Chl 40:40:20 (black) and Ubb^{+1}/POPG-POPC-Chl 40:40:20 (green) are shown.

FIGURES

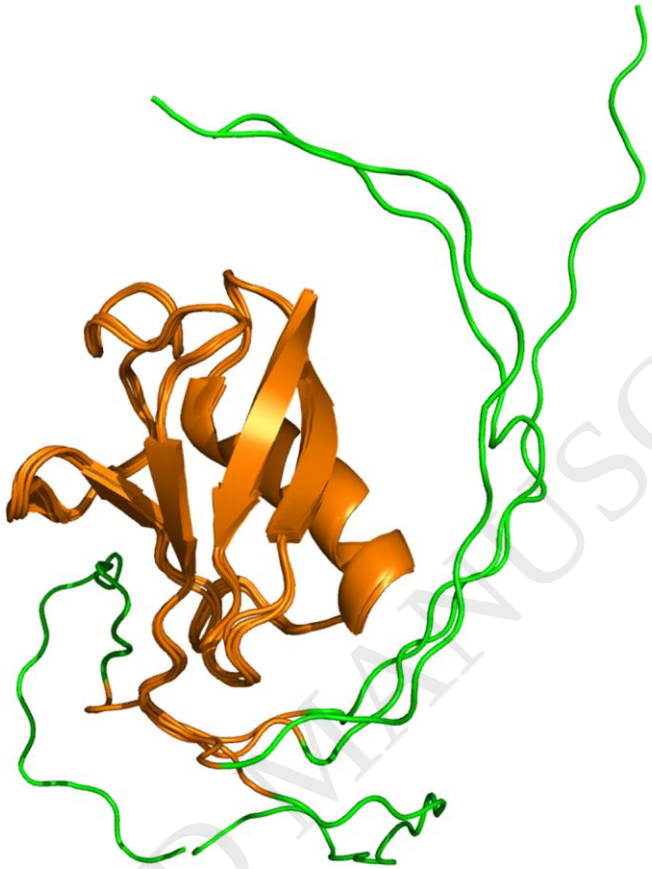

Fig. 1. *Illustration of the structure of Ubb^{+1}.* Cartoon representation of the five lowest energy NMR structures of Ubb^{+1} (PDB 2KX0, [11]). The globular domain is colored in orange, the C-terminal 19-residue fragment is shown in green. The eight exogenous N-terminal residues are not displayed as they are absent in our Ubb^{+1} construct.

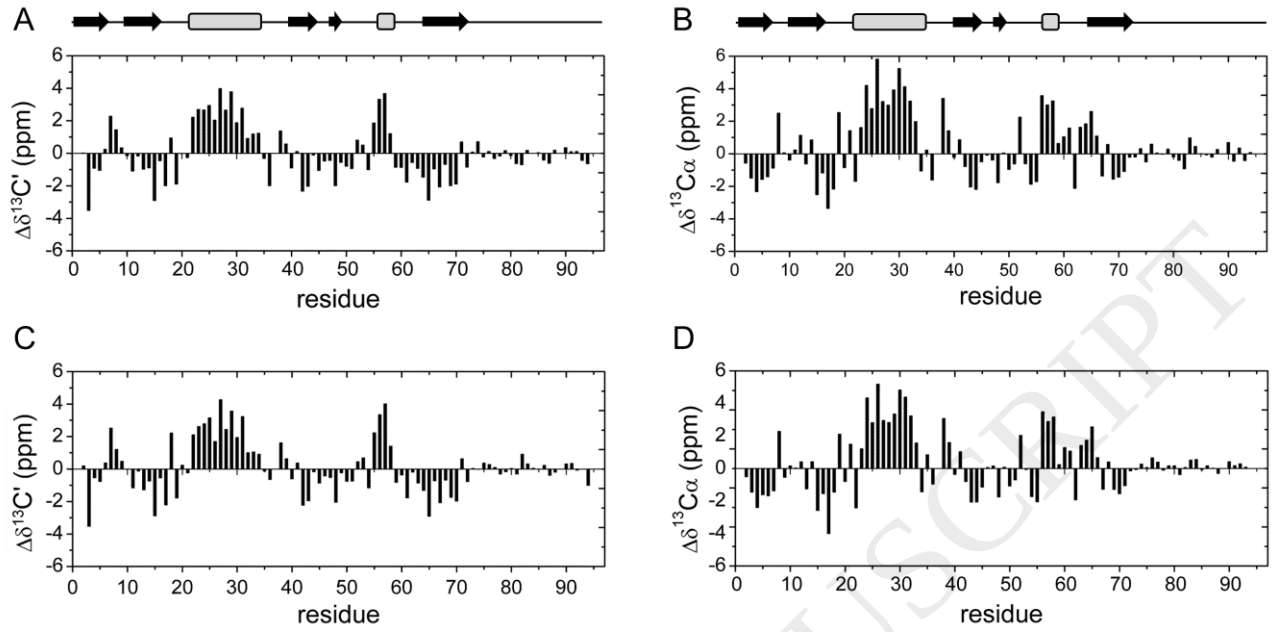

Fig. 2. *Analysis of Ubb^{+1} chemical shifts*. Secondary ^{13}C' (A) and ^{13}Cα (B) chemical shifts ($\Delta\delta^{13}$C' and $\Delta\delta^{13}$Cα) of Ubb^{+1}, obtained with Camcoil random coil values, are plotted versus the protein sequence. Secondary ^{13}C' (C) and ^{13}Cα (D) chemical shifts ($\Delta\delta^{13}$C' and $\Delta\delta^{13}$Cα) of Ubb^{+1}, obtained with the Neighbor Corrected Structural Propensity Calculator random coil values, are plotted versus the protein sequence.

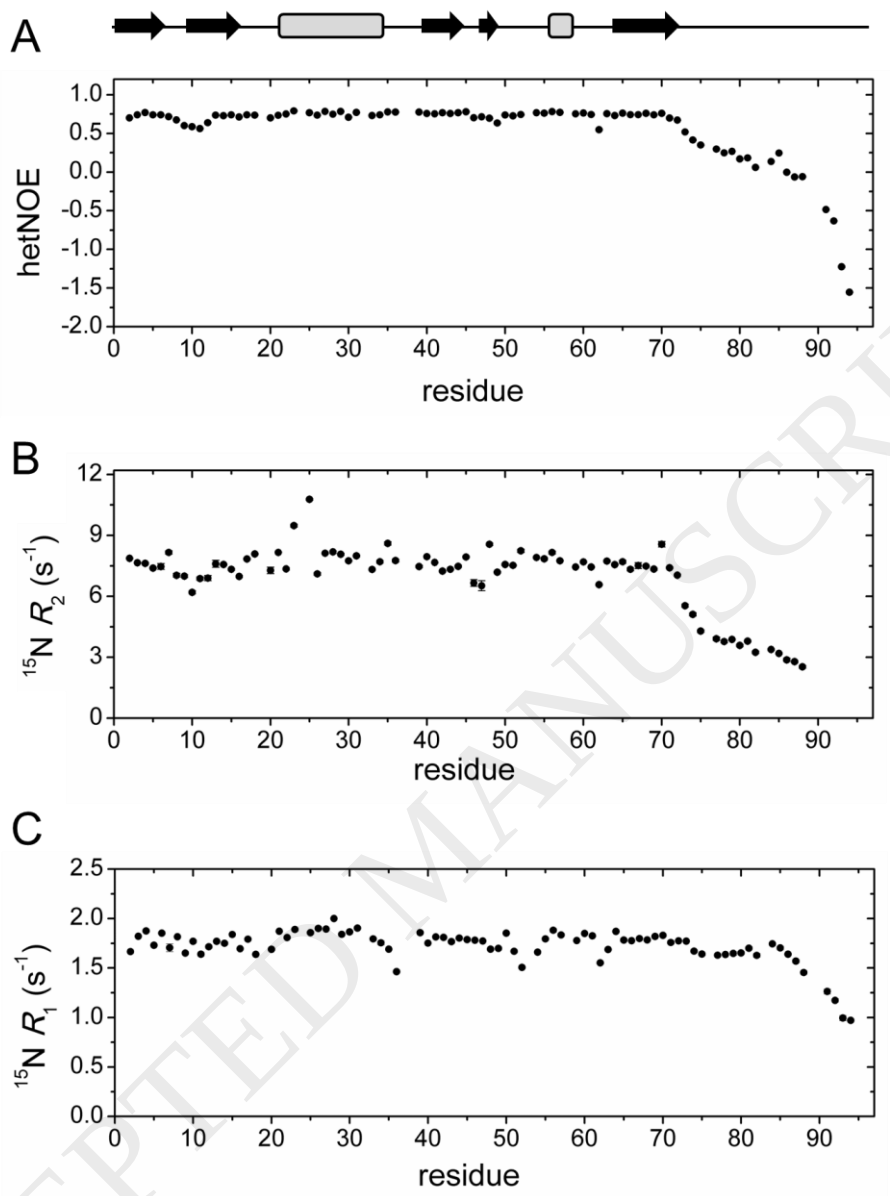

Fig. 3. *Analysis of Ubb^{+1} backbone dynamics*. ^{15}N–spin relaxation rates of [^{15}N]Ubb^{+1} are shown as a function of residue number: A) steady-state {^{1}H}^{15}N heteronuclear NOE (hetNOE); B) R_2 and C) R_1. Residues affected by signal overlap or with insufficient signal-to-noise ratio were excluded from the analysis.

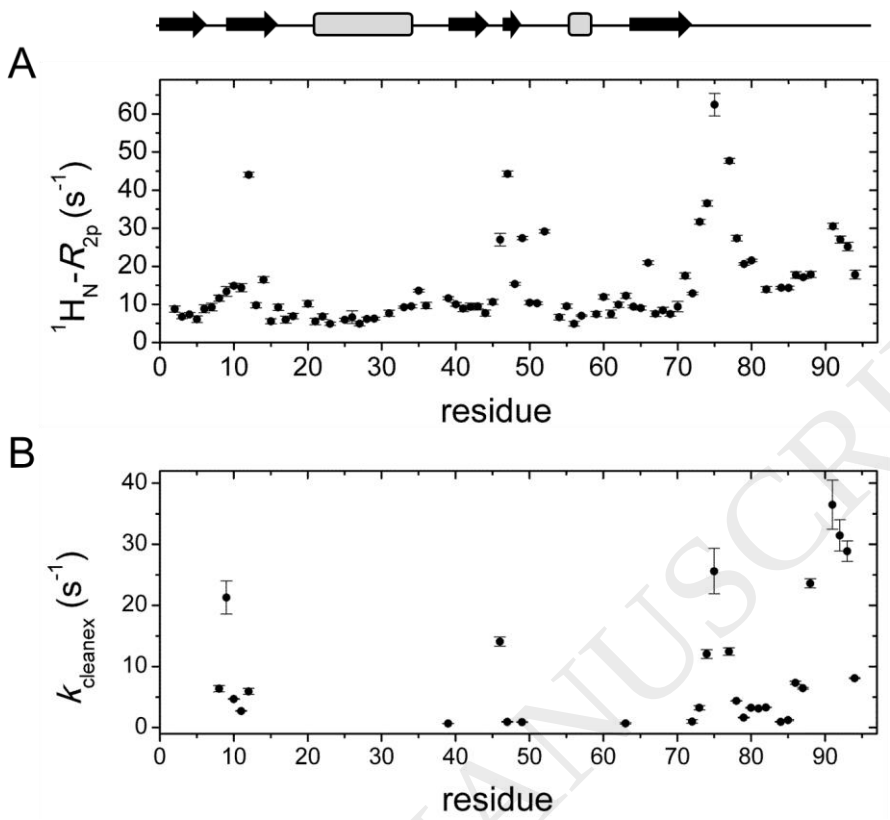

Fig. 4. *Solvent accessibility of Ubb^{+1}.* The solvent exposure of Ubb^{+1} has been probed by solvent PRE (A) or by measurement of water-amide proton exchange rates (B). In A) the ^1H_N-R_{2p} rates of Ubb^{+1} obtained with 2 mM gadodiamide are plotted as a function of protein sequence. In B) the water-amide proton exchange rates (*k*) measured through a CLEANEX-PM-FHSQC experiment are reported versus the protein sequence. Error bars are standard errors obtained from data fitting. Residues affected by signal overlap or with insufficient signal-to-noise ratio were excluded from the analysis.

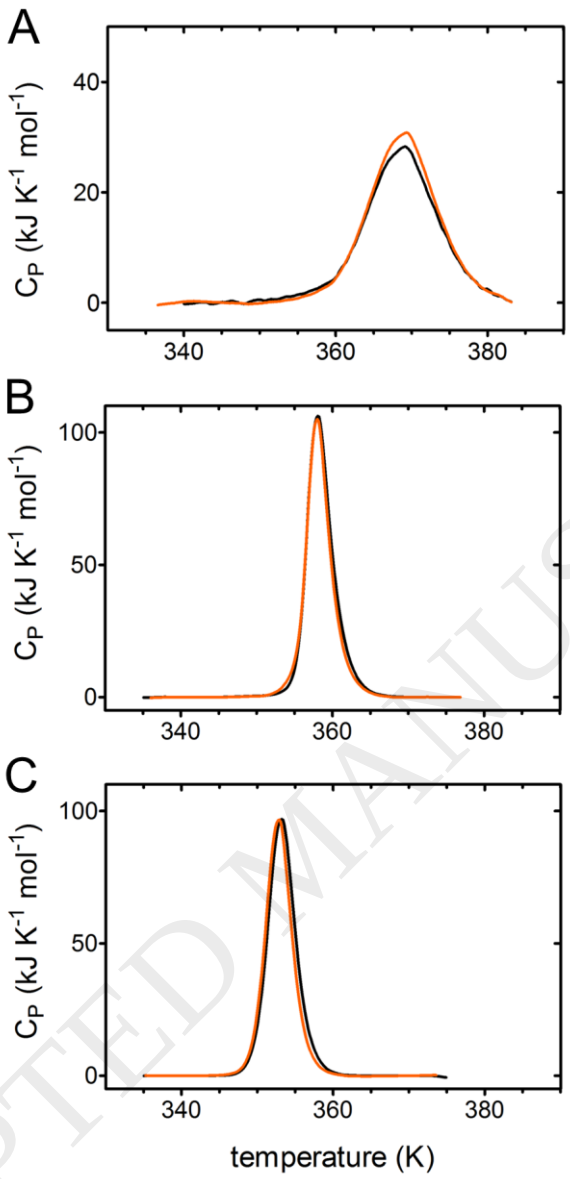

Fig. 5. *Thermal stability measured by calorimetry*. Differential scanning calorimetry thermograms recorded on samples of A) Ub, black, Ubb^{+1}, orange, B) Ub-^{48}Ub, black, Ub-^{48}Ubb^{+1}, orange, C) Ub-^{63}Ub, black, Ub-^{63}Ubb^{+1}, orange. DSC traces are baseline-corrected.

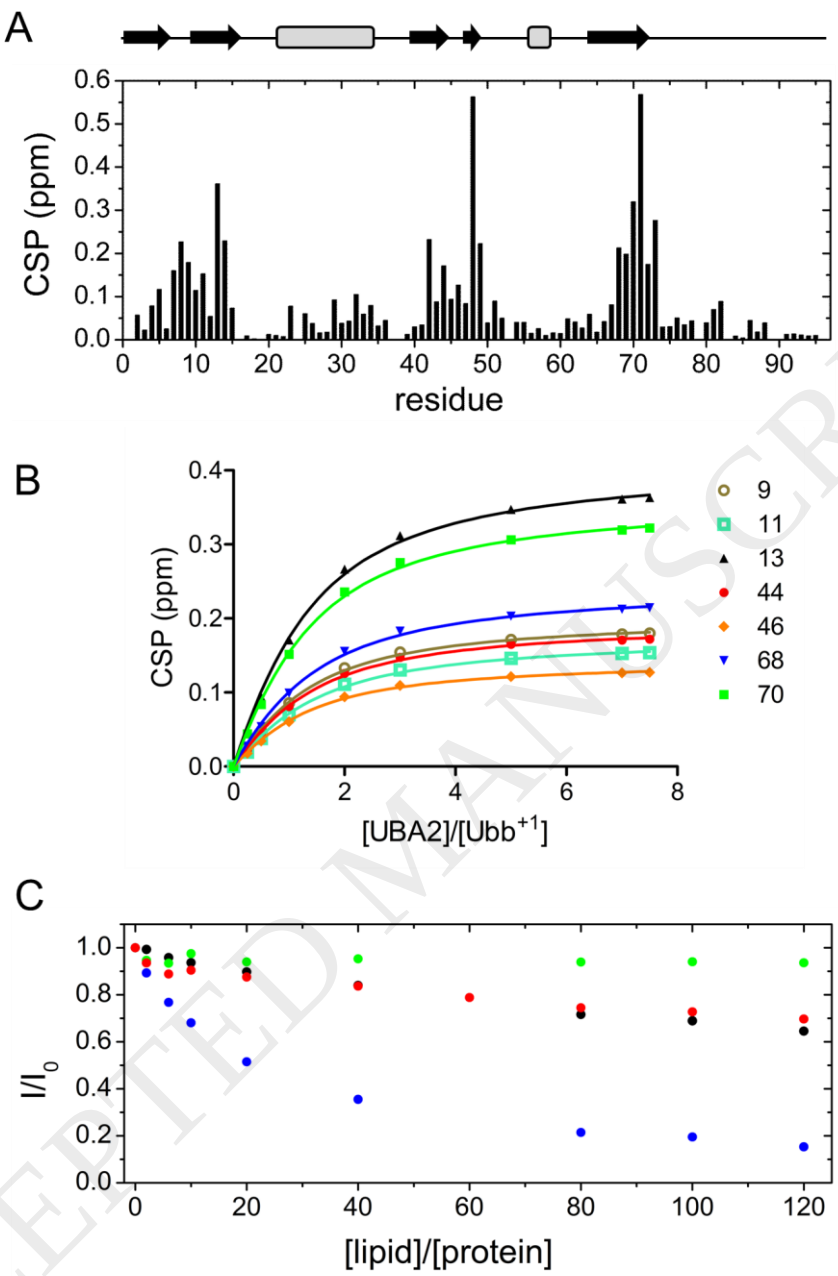

Fig. 6. *Biomolecular interactions of Ubb^{+1}.* A) Plot of the chemical shift perturbations (CSP) determined from ^{1}H,^{15}N-HSQC spectra recorded on [^{15}N]Ubb^{+1} in the presence of (HHR23A)UBA2 at 1:7 molar ratio and in the absence of UBA2. B) Binding isotherms for selected Ubb^{+1} residues based on CSP data from a UBA2/ Ubb^{+1} NMR titration experiment. C) Binding of Ubb^{+1} or Ub to liposomes monitored through analysis of protein ^{1}H signal intensity loss as a function of total lipids to protein molar ratio. Titration data for Ub/POPG-Chl 80:20 (blue), Ubb^{+1}/POPG-Chl 80:20 (red), Ub/POPG-POPC-Chl 40:40:20 (black) and Ubb^{+1}/POPG-POPC-Chl 40:40:20 (green) are shown.